A Thesis for the degree of Doctor of Philosophy

Glycan changes in the olfactory mucosa of rats with experimental autoimmune encephalomyelitis

Department of Veterinary Medicine

GRADUATE SCHOOL
JEJU NATIONAL UNIVERSITY

Changnam Park

2020. 8.

Glycan changes in the olfactory mucosa of rats with experimental autoimmune encephalomyelitis

Changnam Park
(Supervised by Professor Taekyun Shin)

A thesis submitted in partial fulfillment of the requirement for the degree of Doctor of Philosophy in Veterinary Medicine

2020. 6.

This thesis has been examined and approved.

Thesis director, Taeyoung Kang, Ph.D., Jeju National University

Jeongtae Kim, Ph.D., Kosin University

Kwang-Hyup Lee, Ph.D., Seowon Animal Hospital

Hyoung-seok Yang, Ph.D., Veterinary Research Institute,
Jeju Special Self-Governing Province

Taekyun Shin, Ph.D., Jeju National University

Department of Veterinary Medicine
GRADUATE SCHOOL
JEJU NATIONAL UNIVERSITY

CONTENTS

List of Abbreviations

BSL-I	*Bandeiraea simplicifolia* lectin-I
BSL-II	*Bandeiraea simplicifolia* lectin-II
CNS	central nervous system
DBA	*Dolichos biflorus* agglutinin
EAE	experimental autoimmune encephalomyelitis
Iba-1	ionized calcium-binding adaptor molecule-1
LCA	*Lens culinaris* agglutinin
MBP	myelin basic protein
OMP	olfactory marker protein
PBS	phosphate-buffered saline
PGP 9.5	protein gene product 9.5
PI	post-immunization
VVA	*Vicia villosa* agglutinin

List of Figures

List of Tables

General Introduction

Main olfactory and vomeronasal system anatomy

Olfaction involves perception of odorant molecules by the main olfactory system and vomeronasal system and is essential for mammalian social communication and survival (Baum and Cherry, 2015). The olfactory epithelium of the main olfactory system detects odor and covers one-third of the posterior nasal septum and ethmoid turbinate in the nasal cavity (Park et al., 2015). It consists of the supporting cells, basal cells and olfactory sensory neurons.

The vomeronasal system perceives specific environmental compounds, such as pheromones. The vomeronasal organ, located below the nasal septum, is composed of epithelium on the medial surface (Park et al., 2014). Olfactory sensory neurons and vomeronasal sensory neurons sense odorants via apical dendrites and transmit the chemical information to the main olfactory bulb and accessory olfactory bulb through axons (Lledo et al., 2005). The olfactory pathway involves the transmission of odorant signals from the anterior olfactory nucleus to the piriform cortex, olfactory tubercle and anterior cortical amygdala (Figure 1) (Breer et al., 2006).

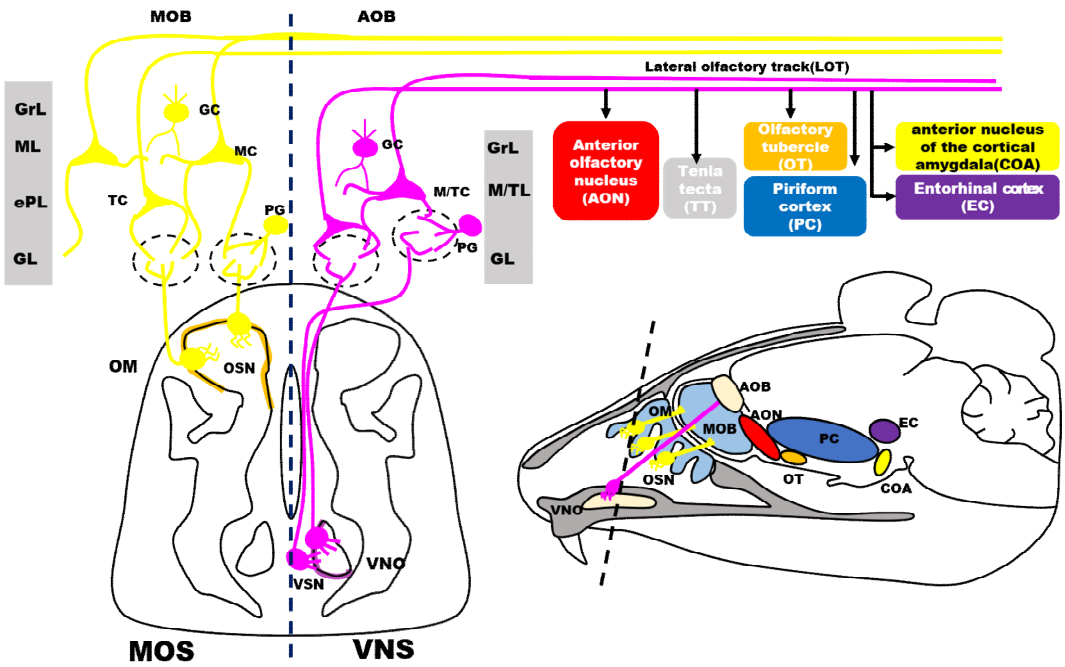

Figure 1. Transduction of olfactory signals. The olfactory mucosa and vomeronasal organ perceive odorant molecules and transmit chemical information to the main olfactory bulb and accessory olfactory bulb, respectively. AON, anterior olfactory nucleus; AOB, accessory olfactory bulb; COA, anterior nucleus of the cortical amygdala; EC, entorhinal cortex; ePL, external plexiform layer; GC, granule cell; GL, glomerular layer; GrL, granule cell layer; MC, mitral cell; ML, mitral cell layer; M/TC, mitral/tufted cell; M/TL, mitral/tufted cell layer; MOB, main olfactory bulb; MOS, main olfactory system; LOT, lateral olfactory track; OM, olfactory mucosa; OSN, olfactory sensory neuron; OT, olfactory tubercle; PC, piriform cortex; PG, periglomerular cell; VNO, vomeronasal organ; VNS, vomeronasal system; VSN, vomeronasal sensory neuron.

Glycans and olfactory function

Glycans are carbohydrate chains that are classified according to their molecular structure, sugar composition and binding specificity (Yamanishi et al., 2007) to monosaccharides such as N-acetylglucosamine, mannose, N-acetylgalactosamine, galactose, and fucose (Rudiger and Gabius, 2001).

Glycans in the olfactory system regulate the development and proliferation of olfactory sensory neurons, synapse formation and odorant signal processing (Plendl and Sinowatz, 1998). Glycans are expressed in a species, cell-type and developmental-specific pattern (Kondoh et al., 2018; Salazar et al., 2000). For example, glycans recognized by *Dolichos biflorus* agglutinin (DBA) appear in undifferentiated olfactory epithelium and disappear after maturation (Plendl and Schmahl, 1988). *Bandeiraea simplicifolia* lectin-I (BSL-I), which has binding specificity for N-acetylgalacosamine, is expressed in rat anterior accessory olfactory bulb after birth, but not during embryogenesis (Ichikawa et al., 1994). Glycans with similar binding specificity may show different expression patterns (Figure 2) (Plendl and Sinowatz, 1998).

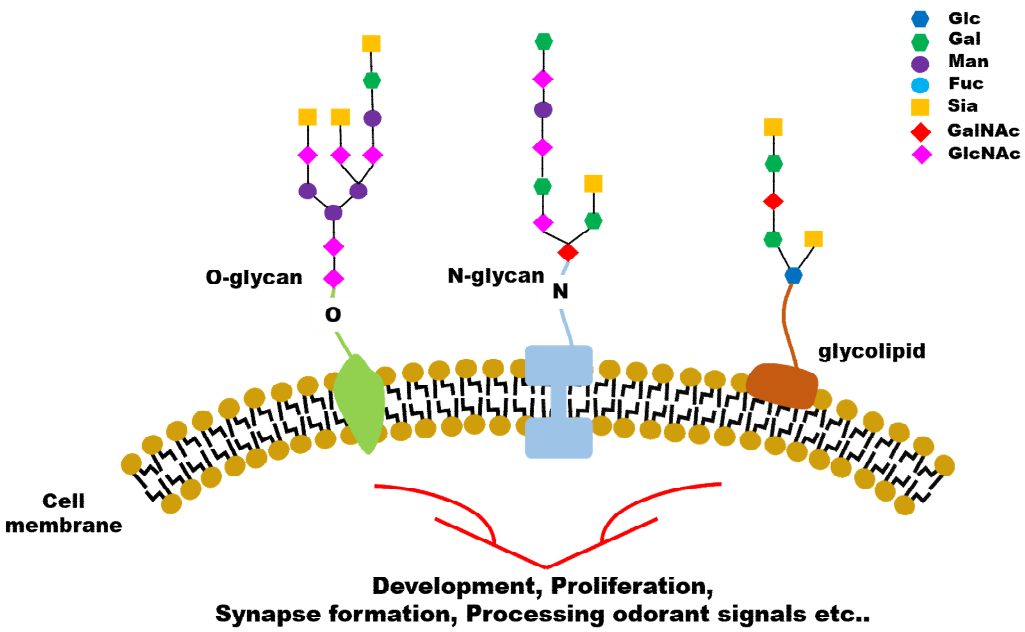

Figure 2. Glycans and olfactory function. Glycans in the olfactory system are involved in neuronal development, proliferation and odorant signal processing.

Neuroinflammation and glycan changes

Glycans are regulated by neuroinflammation. Amyloid-β25-35 injection in rats induces release of neurotoxic-inflammatory cytokines and upregulates mucin-type O-glycosylated proteins and 9-O-acetylated sialic acid moieties in the hippocampus (Limon et al., 2011). Hyperglycemia contributes to optic system inflammation, which causes overexpression of N-glycosylation in the retinal vessel (Liu et al., 2016). In ischemic stroke, immunoglobulin G functionality is altered by lowering galactosylation and sialylation (Liu et al., 2018).

Neuroinflammation and olfaction

Olfactory dysfunction is one of early pathological features of neuroinflammation (Doty, 2017). Some animal models of neuroinflammatory disease, such as Niemann–Pick type C1 mutant mice and APP/PS1 transgenic mice, show the infiltration of macrophages and T-cells in olfactory mucosa and olfactory bulb (Hovakimyan et al., 2013; Yao et al., 2017). Neuroinflammation in central nervous system (CNS) leads to the migration of inflammatory cells through the olfactory nerve (Kim et al., 2018) and the stimulation of immunocytes by CNS inflammatory cytokines from the cerebrospinal fluid and blood circulation (Chen et al., 2015). We postulate that neuroinflammation in experimental autoimmune encephalomyelitis (EAE)-affected rats influences glycan changes in the olfactory system (Figure 3).

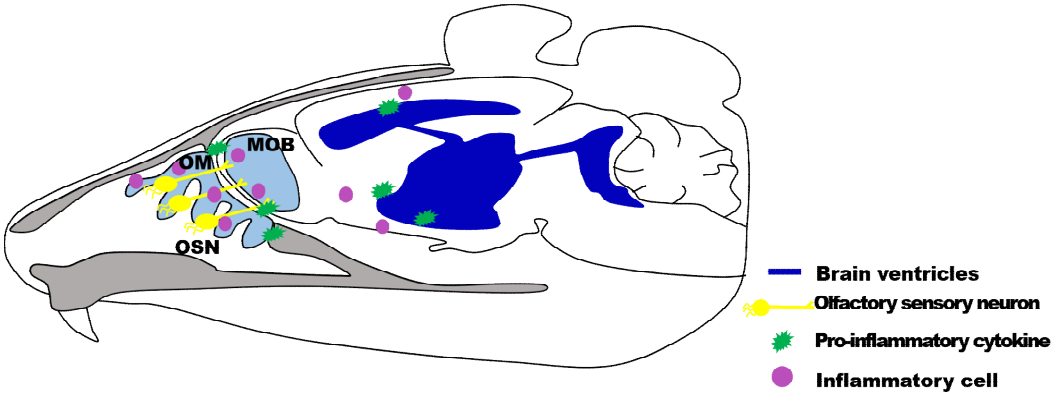

Figure 3. The effects of neuroinflammation in the olfactory system. CNS inflammation affects the olfactory system through migration of inflammatory cells and the stimulation of immunocytes by proinflammatory cytokines.

References

Baum, M.J., Cherry, J.A., 2015. Processing by the main olfactory system of chemosignals that facilitate mammalian reproduction. Horm Behav. 68**,** 53-64.

Breer, H., Fleischer, J., Strotmann, J., 2006. The sense of smell: multiple olfactory subsystems. Cell Mol Life Sci. 63**,** 1465-75.

Chen, L., Elias, G., Yostos, M.P., Stimec, B., Fasel, J., Murphy, K., 2015. Pathways of cerebrospinal fluid outflow: a deeper understanding of resorption. Neuroradiology. 57**,** 139-47.

Doty, R.L., 2017. Olfactory dysfunction in neurodegenerative diseases: is there a common pathological substrate? Lancet Neurol. 16**,** 478-88.

Hovakimyan, M., Meyer, A., Lukas, J., Luo, J., Gudziol, V., Hummel, T., Rolfs, A., Wree, A., Witt, M., 2013. Olfactory deficits in Niemann-Pick type C1 (NPC1) disease. PLoS One. 8**,** e82216.

Ichikawa, M., Takami, S., Osada, T., Graziadei, P.P., 1994. Differential development of binding sites of two lectins in the vomeronasal axons of the rat accessory olfactory bulb. Brain Res Dev Brain Res. 78**,** 1-9.

Kim, J., Choi, Y., Ahn, M., Jung, K., Shin, T., 2018. Olfactory Dysfunction in Autoimmune Central Nervous System Neuroinflammation. Mol Neurobiol. 55**,** 8499-508.

Kondoh, D., Sasaki, M., Kitamura, N., 2018. Age-dependent decrease in glomeruli and receptor cells containing alpha1-2 fucose glycan in the mouse main olfactory system but not in the vomeronasal system. Cell Tissue Res. 373, 361-6.

Limon, I.D., Ramirez, E., Diaz, A., Mendieta, L., Mayoral, M.A., Espinosa, B., Guevara, J., Zenteno, E., 2011. Alteration of the sialylation pattern and memory deficits by injection of Abeta(25-35) into the hippocampus of rats. Neurosci Lett. 495, 11-6.

Liu, D., Zhao, Z., Wang, A., Ge, S., Wang, H., Zhang, X., Sun, Q., Cao, W., Sun, M., Wu, L., Song, M., Zhou, Y., Wang, W., Wang, Y., 2018. Ischemic stroke is associated with the pro-inflammatory potential of N-glycosylated immunoglobulin G. J Neuroinflammation. 15, 123.

Liu, K., Liu, H., Zhang, Z., Ye, W., Xu, X., 2016. The role of N-glycosylation in high glucose-induced upregulation of intercellular adhesion molecule-1 on bovine retinal endothelial cells. Acta Ophthalmol. 94, 353-7.

Lledo, P.M., Gheusi, G., Vincent, J.D., 2005. Information processing in the mammalian olfactory system. Physiol Rev. 85, 281-317.

Park, C., Ahn, M., Lee, J.Y., Lee, S., Yun, Y., Lim, Y.K., Taniguchi, K., Shin, T., 2014. A morphological study of the vomeronasal organ and the accessory olfactory bulb in the Korean roe deer, Capreolus

pygargus. Acta Histochem. 116, 258-64.

Park, C., Ahn, M., Kim, J., Kim, S., Moon, C., Shin, T., 2015. Histological and lectin histochemical studies on the olfactory mucosae of the Korean roe deer, Capreolus pygargus. Tissue Cell. 47, 221-7.

Plendl, J., Schmahl, W., 1988. Dolichos biflorus agglutinin: a marker of the developing olfactory system in the NMRI-mouse strain. Anat Embryol (Berl). 177, 459-64.

Plendl, J., Sinowatz, F., 1998. Glycobiology of the olfactory system. Acta Anat (Basel). 161, 234-53.

Rudiger, H., Gabius, H.J., 2001. Plant lectins: occurrence, biochemistry, functions and applications. Glycoconj J. 18, 589-613.

Salazar, I., Sanchez-Quinteiro, P., Lombardero, M., Cifuentes, J.M., 2000. A descriptive and comparative lectin histochemical study of the vomeronasal system in pigs and sheep. J Anat. 196 (Pt 1), 15-22.

Yamanishi, Y., Bach, F., Vert, J.P., 2007. Glycan classification with tree kernels. Bioinformatics. 23, 1211-6.

Yao, Z.G., Hua, F., Zhang, H.Z., Li, Y.Y., Qin, Y.J., 2017. Olfactory dysfunction in the APP/PS1 transgenic mouse model of Alzheimer's disease: Morphological evaluations from the nose to the brain. Neuropathology. 37, 485-494.

Glycan changes in the olfactory mucosa of rats with experimental autoimmune encephalomyelitis

1. Abstract

Glycans are components of glycoconjugates and function in odorant recognition and cell signaling in the olfactory mucosa. However, little is known about glycan expression in the olfactory mucosa in the presence of neuroinflammatory disorders, which can influence olfaction. We evaluated the changes in glycan in the olfactory mucosa of rats with EAE by histochemical analyses of 21 lectins. In the olfactory mucosa of normal control rats, 16 lectins bound to olfactory sensory neurons, supporting cells, basal cells, nerve and Bowman's glands, and their expression did not significantly change during the course of EAE. In rats with paralytic-stage EAE, five lectins showed different reactivities with the olfactory mucosa compared to those of normal control rats. Of them, BSL-II and BSL-I showed transiently downregulated binding to olfactory sensory neurons and supporting cells in rats with EAE. The reactivities of *Lens culinaris* agglutinin (LCA) for the basement membrane, *Vicia villosa* agglutinin (VVA) for Bowman's glands and DBA for all nuclei were upregulated in the olfactory mucosa of EAE rats. These results suggest that BSL-II-binding N-acetyl-glucosamine and BSL-I-binding N-acetyl-galactose are involved in transient olfactory dysfunction in EAE, which may hamper odor perception and/or signal processing in olfactory sensory neurons.

Key words: Experimental autoimmune encephalomyelitis, olfactory mucosa, lectin, glycan

2. Introduction

Glycans are carbohydrate moieties of glycoconjugates that play crucial roles in cell/cell interactions, synapse formation, and cell proliferation in the olfactory system (Plendl and Sinowatz, 1998). In the olfactory system, glycans are differentially expressed according to development stage (Plendl and Schmahl, 1988), aging (Kondoh et al., 2018), and species (Salazar et al., 2000); therefore, glycan expression analysis is important for understanding the biological significance of changes in the olfactory system. Plant lectin histochemical analyses are useful diagnostic tools for the investigation of glycan expression levels in the olfactory system (Lipscomb et al., 2003).

The olfactory mucosa lines the ethmoturbinates in the nasal cavity and plays an important role in olfaction, which is essential for social interaction and reproductive behavior (Patel and Pinto, 2014). The olfactory mucosa is composed of olfactory sensory neurons, supporting cells, basal cells, and Bowman's glands (Ichikawa et al., 1994; Oikawa et al., 2001; Saito et al., 1994). Each of these components harbors a variety of glycans intracellularly or in the extracellular matrix (Kondoh et al., 2018; Melgarejo Moreno et al., 1998; Plendl and Sinowatz, 1998).

Olfactory dysfunction is an early sign of neuroinflammation, such as that seen, for example, in multiple sclerosis patients (Caminiti et al., 2014; Kim et al., 2018; Shin et al., 2018). EAE is an animal model of human multiple sclerosis, and is characterized by infiltration of the CNS by autoreactive T cells and macrophages (Shin et al., 2012). We previously reported that inflammation, microgliosis, and astrogliosis occur in the olfactory mucosa and the olfactory bulb of rats and mice with EAE (Kim et al., 2018; Kim et al., 2019). Because glycan expression in the nervous system is altered by inflammation (Limon et al., 2011; Ramos-Martinez et al., 2018), we postulated that neuroinflammation influences glycan expression in the olfactory mucosa in rats with EAE. In this study, we evaluated glycan expression in the olfactory mucosa of rats with EAE by performing histochemical analysis on 21 lectins.

3. Materials and Methods

3.1. Animals

Male Sprague-Dawley rats (8-10 weeks of age, n = 15) were obtained from Orient Bio Inc. (Gyeonggi-do, Republic of Korea), and were maintained in our animal facility. All experimental procedures were conducted in accordance with the Guidelines for the Care and Use of Laboratory Animals of Jeju National University (permission no. 2017-0019). The animal protocols also conformed to current international laws and the policies of the Guide for the Care and Use of Laboratory Animals of the United States National Institutes of Health (NIH; publication no. 85-23, 1985, revised 1996). Every effort was made to minimize the number of animals used and their suffering.

3.2. Induction of EAE

The footpads of both hind feet of the rats were inoculated with 100 μL of an emulsion containing an equal volume of guinea pig myelin basic protein (MBP) (1 mg/mL) and complete Freund's adjuvant supplemented with 5 mg/mL *Mycobacterium tuberculosis* H37Ra (Difco Laboratories Inc., Detroit, MI, USA). Pertussis toxin (500 ng; List Biological Laboratories, Inc., Campbell, CA, USA) was intraperitoneally injected into the rats at days 0 and 2 post immunization (PI). Rats were observed daily post-immunization for clinical signs of EAE. EAE progression was behaviorally divided into the following seven stages: grade 0 (G.0), no signs; G.1, floppy tail; G.2, incomplete hind-limb paralysis;

G.3, hind-limb paralysis; G.4, tetraparesis; G.5, moribund condition or death; and R.0, recovery. We sampled rat tissues at arbitrary intervals to assess whether the paralytic and recovery stages had been reached at days 12-15 PI and days 19-21 PI, respectively.

3.3. Histological Examination

Rats were deeply anesthetized via intra-peritoneal injection of a solution (0.1 mL/100 g body weight) containing ketamine (50 mg/ml, YUHAN, Seoul, Republic of Korea), xylazine (5 mg/ml, KBNP, Gyeonggi-Do, Republic of Korea) and acepromazine (1 mg/ml, SAMU MEDIAN, Chungcheongnam-Do, Republic of Korea). Rats with EAE were perfused with 4% (v/v) paraformaldehyde in phosphate-buffered saline (PBS; pH 7.2). To examine the olfactory mucosa of rats, the heads of rats fixed in 4% paraformaldehyde, were immersed in a large volume of formic acid-sodium citrate solution. The solution was changed daily until decalcification was complete, and the heads were processed for paraffin embedding.

3.4. Immunohistochemistry and immunofluorescence

Immunohistochemistry was performed using a commercial avidin-biotin complex kit (Vectastain® Elite ABC Kit; Vector Laboratories, Burlingame, CA, USA), as in our previous study (Ahn et al., 2012). Briefly, after incubating with normal goat serum (10% [v/v] in PBS), the sections were incubated with rabbit anti-ionized calcium-binding adaptor molecule-1 (Iba-1) (1:1,000; 019-19741, Lot. LKH4161; Wako Pure Chemical Industries, Ltd. Osaka, Japan) for 1 h at room temperature.

Following three washes in PBS, the signal was developed using a diaminobenzidine substrate kit.

To identify glycans in olfactory sensory neurons, we performed double immunofluorescence staining for olfactory marker protein (OMP) and protein gene product 9.5 (PGP 9.5) as markers of olfactory sensory neurons (Kim et al., 2019). Sections were incubated with goat anti-OMP (1:500, SC-49070, Lot no. B2714; Santa Cruz Biotechnology, Santa Cruz, CA, USA) and mouse anti-PGP 9.5 (1:500, ab72911, Lot no. GR251185-1, abcam, Cambridge, United Kingdom), and visualized using a fluorescein isothiocyanate-conjugated anti-goat IgG (1:50, Sigma-Aldrich) and fluorescein isothiocyanate-conjugated anti-mouse IgG (1:50, Sigma-Aldrich). The sections were washed three times and then incubated with biotinylated lectins, including BSL-I and -II, which showed positive reactions in the olfactory sensory neuron layer. The slides were incubated with tetramethylrhodamine isothiocyanate-labeled streptavidin (1:500, Zymed, San Francisco, CA, USA). Images were captured using an Olympus BX-51 fluorescence microscope (Olympus Corp., Tokyo, Japan) and merged using Adobe Photoshop (Adobe Systems, San Jose, CA).

3.5. Lectin histochemistry

The BK-1000, BK-2000, and BK-3000 Lectin-Screening Kits (Vector Laboratories Burlingame, CA, USA) were used in this study. Lectins are classified into the following six groups according to their binding specificity and inhibitory sugar: N-acetylglucosamine, mannose, galactose, N-acetylgalactosamine, fucose, and complex type N-glycans (Table

1). Histochemical analyses of lectins were performed as described previously (Lee et al., 2016; Shin et al., 2017). In brief, paraffin-embedded ethmoturbinates (5 μm thickness) were counterstained with hematoxylin and mounted on slide glasses. The sections were rehydrated by an ethanol series. Endogenous peroxidase activity was blocked using 0.3% H_2O_2 in methanol for 30 min. After three washes with PBS, the sections were incubated with 1% bovine serum albumin to block non-specific reactivity. The sections were rinsed with PBS and incubated with the 21 biotinylated lectins at 4°C overnight. The signal was developed using a diaminobenzidine substrate kit (Vector Laboratories). For the negative control, we (1) omitted a primary reagent and (2) pre-incubated lectins with inhibitory sugar (0.2-0.5 M in Tris buffer) following the methods of previous studies (Kaltner et al., 2007; Lee et al., 2016).

Table 1 Plant lectins used in this study

Lectin abbreviation	Source	Concentration (mg/ml)	Inhibitor or eluting sugar*
N-acetylglucosamine binding lectins			
s-WGA	Succinylated *Triticum vulgaris*	1.0×10^{-2}	0.2 M GlcNAc
WGA	*Triticum vulgaris*	1.0×10^{-2}	0.2 M GlcNAc
BSL-II	*Bandeiraea simplicifolia*	4.0×10^{-3}	0.2 M GlcNAc
DSL	*Datura stramonium*	4.0×10^{-3}	0.5 M chitin hydrolysate
LEL	*Lycopersicon esculentum*	2.0×10^{-2}	0.5 M chitin hydrolysate
STL	*Solanum tuberosum*	1.0×10^{-2}	0.5 M chitin hydrolysate
Mannose binding lectins			
ConA	*Canavalia ensiformis*	3.3×10^{-3}	0.2 M MeαMan/0.2 M MeαGlc
LCA	*Lens culinaris*	4.0×10^{-3}	0.2 M MeαMan/0.2 M MeαGlc
PSA	*Pisum sativum*	4.0×10^{-3}	0.2 M MeαMan/0.2 M MeαGlc
N-acetylgalactosamine binding lectins			
VVA	*Vicia villosa*	4.0×10^{-3}	0.2 M GalNAc
DBA	*Dolichos biflorus*	1.0×10^{-2}	0.2 M GalNAc
SBA	*Glycine max*	1.0×10^{-2}	0.2 M GalNAc
SJA	*Sophora japonica*	2.0×10^{-2}	0.2 M GalNAc
BSL-I	*Bandeiraea simplicifolia*	4.0×10^{-3}	0.2 M GalNAc
Galactose binding lectins			
RCA_{120}	*Ricinus communis*	2.0×10^{-3}	0.2 M lactose
Jacalin	*Artocarpus integrifolia*	5.0×10^{-4}	0.2 M melibiose
PNA	*Arachis hypogaea*	4.0×10^{-3}	0.2 M βGal
ECA	*Erythrina cristagalli*	2.0×10^{-2}	0.2 M lactose
Complex type N-glycan (Complex oligosaccharide) binding lectins			
PHA-E	*Phaseolus vulgaris*	5.0×10^{-3}	0.1 M acetic acid
PHA-L	*Phaseolus vulgaris*	2.5×10^{-3}	0.1 M acetic acid
Fucose binding lectins			
UEA-I	*Ulex europaeus*	2.0×10^{-2}	0.1 M L-fucose

Gal, galactose; GalNAc, N-acetylgalactosamine; GlcNAc, N-acetylglucosamine; MeαMan, α-Methylmannoside; MeαGlc, α-Methylglucoside

3.6. Quantification of lectin and/or antibody-positive area

Prior to semi-quantitative analysis, we photographed lectin and/or antibody-positive sections (n = 5 per group) using a digital camera (ProgRes C5, Olympus DP72; Olympus Corp., Tokyo, Japan) attached to a light microscope (Olympus BX53/U-LH 100HG; Olympus Corp.). Six points (left and right nasal septum, dorsal roof of the nasal cavity, and ethmoturbinates) of the olfactory mucosa and three sections of spinal cord (cervical, thoracic and lumbar spine) were photographed in each slide. The lectin and/or antibody-positive area was semi-quantified using ImageJ software (NIH, Bethesda, MD) (Figure 4). Finally, the ratio of the lectin and/or antibody-positive area to the total area [(positive area/total area) × 100] was calculated.

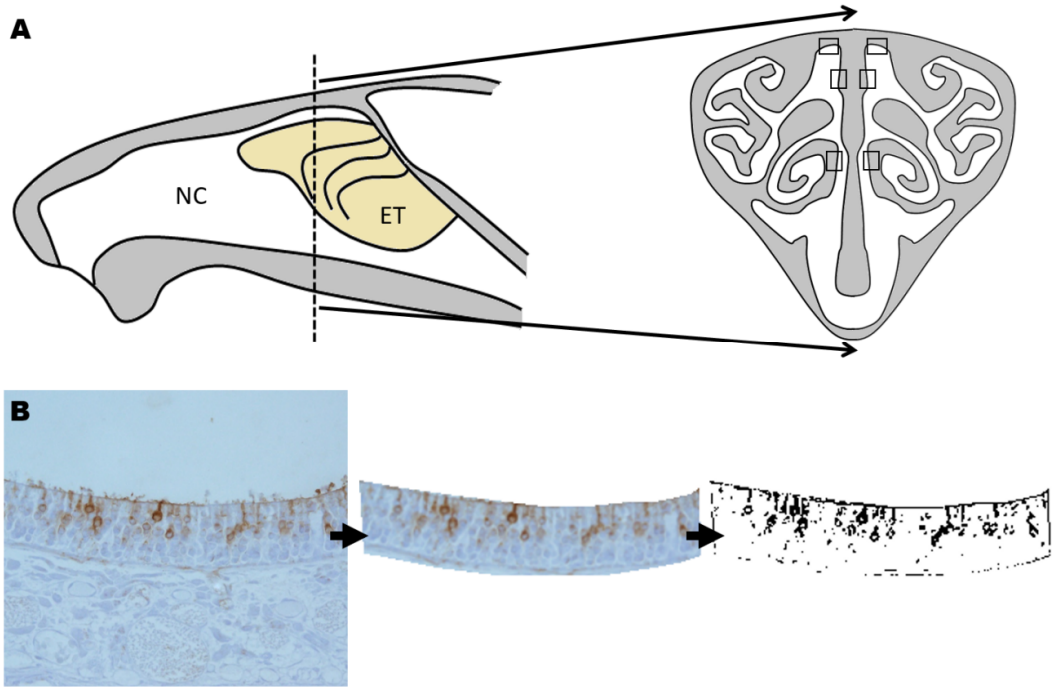

Figure 4. Measurement of the lectin and/or antibody-positive area. (A) Coronal-plane image of the rat nasal cavity. (B) Image processing to measure the lectin-positive area. NC, nasal cavity; ET, ethmoid turbinate; dotted line, position of the coronal section; quadrangle, area of measurement.

3.7. Statistical analysis

Data represent means ± standard errors of the mean of three independent experiments. We performed one-way analysis of variance followed by Tukey's test for multiple comparisons at a significance level of $p < 0.05$.

4. Results

4.1 Behavioral Evaluation after immunization

MBP-immunized rats exhibited floppy tails at around day 11 PI. At days 12-15 PI, clinical signs of EAE progressed to hind-limb paralysis. EAE-affected rats gradually recovered from hind-limb paralysis from days 19-21 PI (Figure 5 and Table 2).

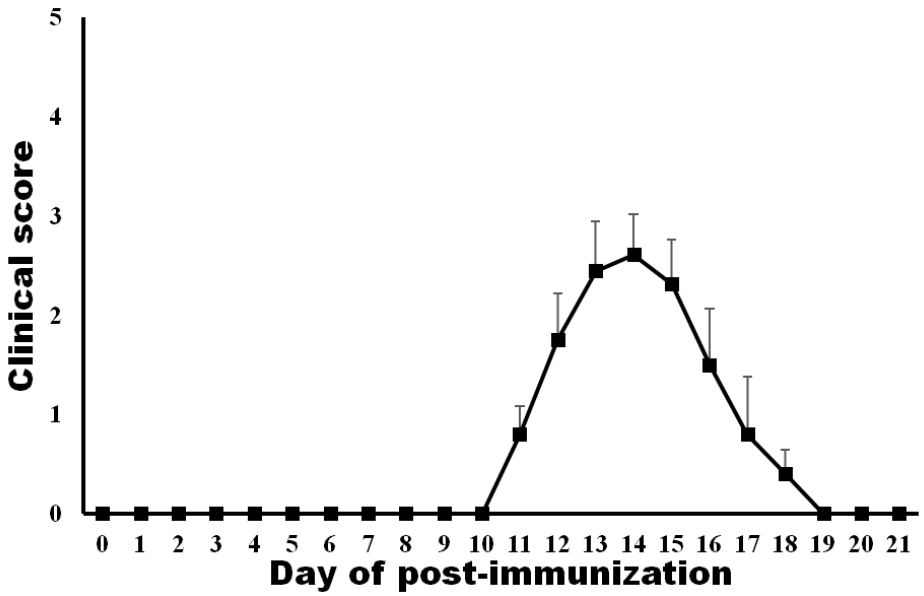

Figure 5. Behavioral evaluation in EAE-affected rats. Immunized rats were observed daily for clinical signs of EAE. The paralytic and recovery stages were reached at days 12-15 and days 19-21 PI, respectively. Data are presented as means ± standard errors of the mean.

Table 2 Summary of clinical use of EAE-affected rats

Group	EAE incidence (paralyzed/total animals)	First onset of paralysis	Average maximum clinical score	Mortality
Normal control	0/5	-	-	0/5
EAE induction	10/10	11.9 ± 0.41	2.75 ± 0.29	0/10

4.2. Histological and immunohistochemical analyses of the spinal cord

In the normal control spinal cord, tissue structure was well-defined (Figure 6A) and Iba-1 reactivity was weak (Figure 6D and 6G, 2.82 ± 0.09%). During paralytic-stage of EAE (days 12-15 PI), many inflammatory cells (arrowheads in Figure 6B) invaded the parenchyma of the spinal cord and immunoreactivity for Iba-1 was sharply increased than those of normal control (Figure 6E and 6G, 7.93 ± 0.38%, $p < 0.001$). In rats with recovery-stage EAE (days 19-21 PI), some inflammatory cells (arrowheads in Figure 6C) still formed a perivascular cuff in the spinal cord , but the degree of Iba-1 immunoreactivity was remarkably reduced compared to those with paralytic-stage EAE (Figure 6F and 6G, 4.74 ± 0.15%, $p < 0.001$).

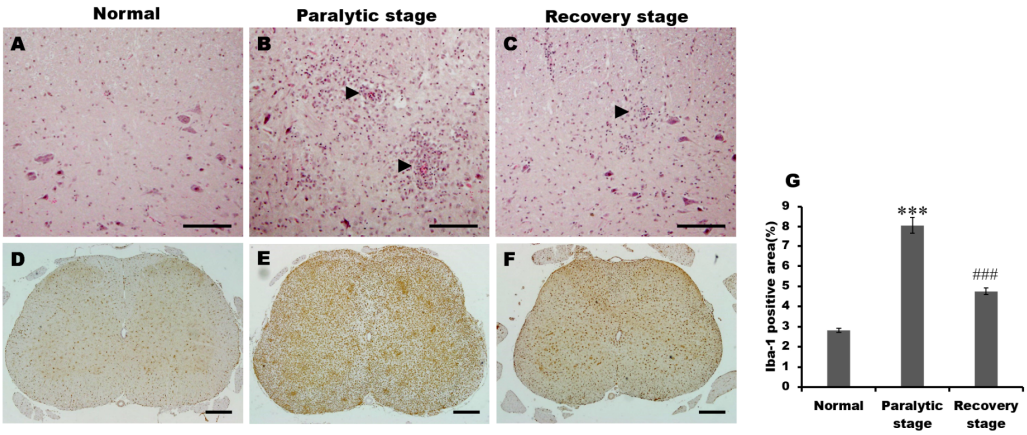

Figure 6. Histological analysis and immunohistochemical staining for Iba-1 in the spinal cord of normal control and EAE-affected rats. (A) No inflammatory response was detected in the spinal cords of normal control rats. (B) Many inflammatory cells (arrowheads) infiltrated into the parenchyma of the spinal cord at the paralytic stage of EAE. (C) At the recovery stage of EAE, some inflammatory lesions (arrowhead) were still observed in the spinal cord. (D-F) Low-magnification of Iba-1 staining in spinal cord of the normal control and EAE-affected rats. (G) A semi-quantitative analysis for Iba-1-positive area of the spinal cord in normal and EAE-affected rats. $^{***}p< 0.001$, vs. normal controls. $^{###}p< 0.001$, vs. paralytic stage. A-C, Hematoxylin and eosin staining. Scale bars in A-C = 50 μm, Scale bars in D-F = 800 μm

4.3. Histological and immunohistochemical analyses of the olfactory mucosa

In the histological aspect, some round cells (arrows in Figure 7B) were detected in the olfactory mucosa of rats with paralytic-stage EAE. There were no significant differences between normal control (Figure 7A) and recovery-stage EAE rat (Figure 7C). Comparing Iba-1 reactivity for the olfactory mucosa of normal control and EAE-affected rats, Iba-1-positive area were increased and abundant Iba-1-positive cells were found in paralytic-stage EAE (Figure 7E and 4G, 8.19 ± 0.47%, $p < 0.01$) than those of normal control (Figure 7D and 4G, 3.23 ± 0.62%). In olfactory mucosa of rats with recovery-stage EAE (days 19-21 PI), Iba-1 reactivity were reduced (Figure 7F and 7G, 4.93 ± 1.16%, $p < 0.05$) than that of rats with paralytic-stage EAE. In double immunofluorescence staining with PGP 9.5 (Figure 7H-7J, green color) and Iba-1 (Figs. 7H-7J, red color) of the olfactory mucosa of normal controls and EAE-affected rats, Iba-1-positive inflammatory cells (arrows in Figure 7I) were examined in EAE-paralytic stage, but not co-localized with PGP 9.5.

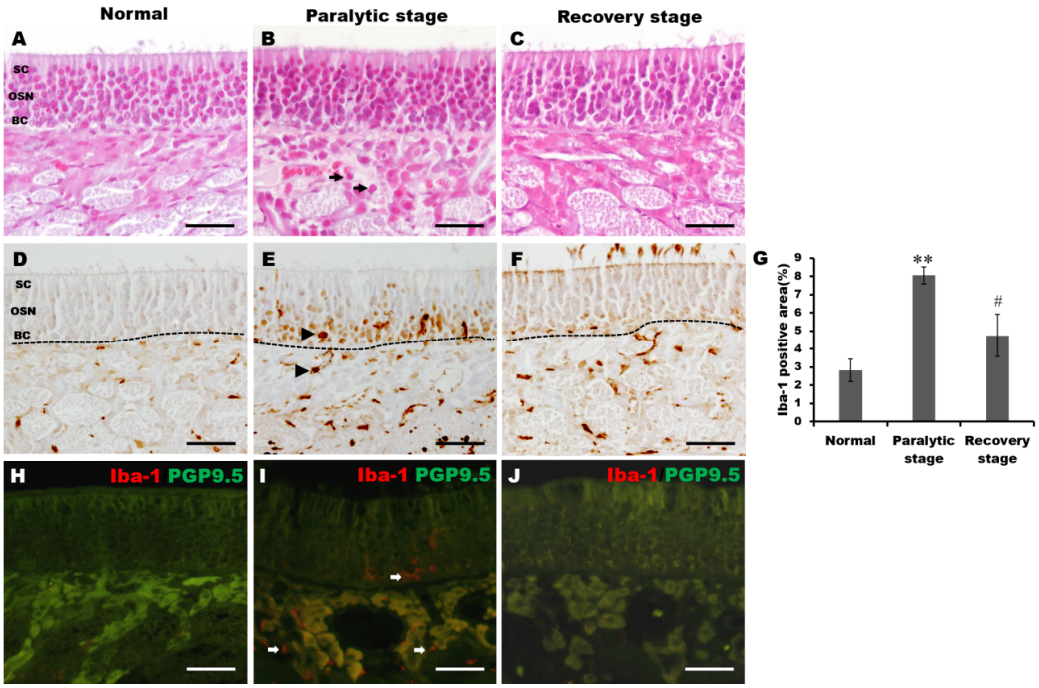

Figure 7. Histological analysis and immunohistochemical staining of Iba-1 in the olfactory mucosa of normal control and EAE-affected rats. (A) Supporting cells (SCs), olfactory sensory neurons (OSNs), and basal cells (BCs) were well arranged in the olfactory epithelium of the normal control. (B) Round-shaped cells (arrows) were found in the lamina propria at the paralytic stage of EAE. (C) Inflammatory cells were rarely detected in the olfactory mucosa at the recovery stage. (D) Weak Iba-1 reactivity was observed in the normal control. (E) However, Iba-1 expression generally increased, with some Iba-1-positive inflammatory cells (arrowheads) invading the olfactory mucosa at the paralytic stage. (F) At the recovery stage, Iba-1 expression was lower than that in the paralytic stage. (G) Semi-quantitative analysis of the Iba-1-positive area of the olfactory mucosa in normal and EAE-affected rats. (H-J) Double immunofluorescence reactivity to anti-PGP 9.5 (green), an olfactory sensory marker, and anti-Iba-1 (red), an inflammatory cell marker, in the olfactory mucosa of normal (H) and EAE-affected rats at the (I) paralytic and (J) recovery stages. Arrows indicate Iba-1-positive inflammatory cells that were not co-localized with PGP 9.5 at the EAE-paralytic stage. $^{**}p< 0.01$, vs. normal control. $^{\#}p< 0.05$, vs. paralytic stage. Scale bars in A-I = 20 μm.

4.4. Lectin histochemistry

4.4.*1*. *BSL-II reactivity is reduced in the olfactory mucosa of EAE-affected rats among N-acetylglucosamine binding lectins*

The perinuclear region of some olfactory sensory neurons and supporting cells was labeled with BSL-II in normal control rats (Figure 8A) but this had disappeared in rats with paralytic-stage EAE (Figure 8B). In rats with recovery-stage EAE, BSL-II weakly bound to some olfactory sensory neurons and supporting cells (Figure 8C). No reactivity for BSL-II was shown in pre-incubation with 0.2 M GlcNAc (Figure 8D). A semi-quantitative comparison (Figure 8E) revealed that the BSL-II-positive area in the olfactory mucosa of rats with paralytic-stage EAE was significantly decreased (1.56 ± 0.38%, $p < 0.001$) compared to that of normal control rats (11.33 ± 1.95%), while the area increased in rats with recovery-stage EAE (7.04 ± 1.37%, $p < 0.05$ vs. paralytic stage; $p > 0.05$ vs. normal; Figure 8E). There were no differences in lectin-binding reactivity with succinylated-wheat germ agglutinin, wheat germ agglutinin, *Datura stramonium lectin*, *Lycopersicon esculentum* lectin, and *Solanum tuberosum* lectin between normal control rats and rats with EAE (Table 3).

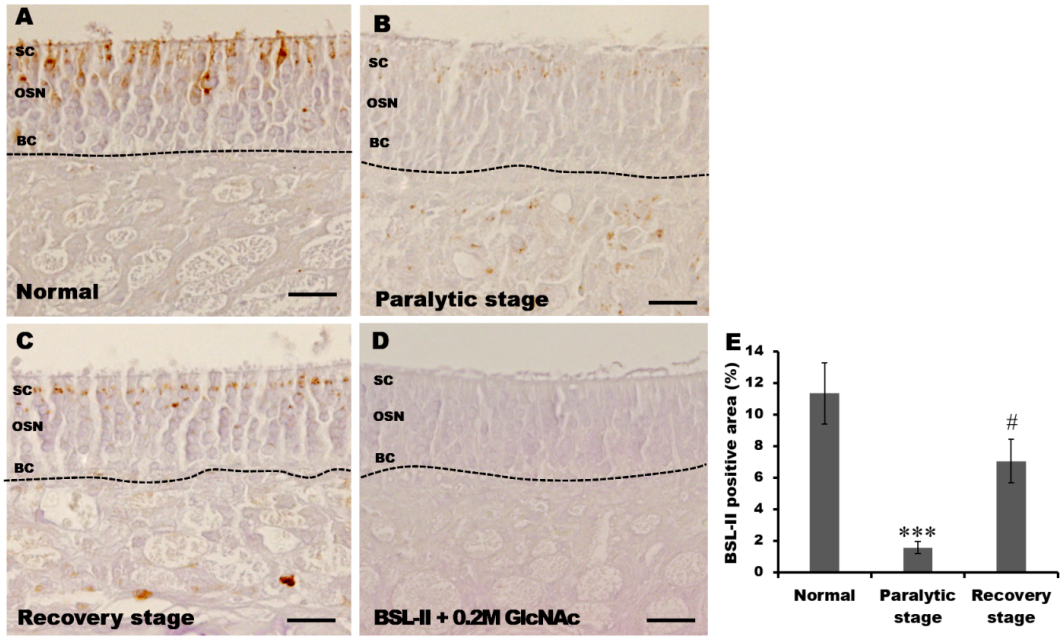

Figure 8. Lectin histochemistry for BSL-II in the olfactory mucosa of (A) normal control, (B) paralytic-stage EAE, and (C) recovery-stage EAE rats. (A) In normal controls, BSL-II reactivity was labeled in some olfactory sensory neurons and supporting cells; (B) however, these labels disappeared at the paralytic stage. (C) Weak BSL-II reactivity was labeled in olfactory sensory neurons and supporting cells in the recovery stage. (D) Pre-incubation with 0.2 M GlcNAc as a negative control. BSL-II reactivity was abolished using inhibitory sugar. (E) Bar graphs show semi-quantitative analysis results for the BSL-II-positive area of the olfactory mucosa in normal control and EAE rats. BSL-II-positive area was measured above the dotted line. $^{**}p < 0.01$ vs. normal control, $^{\#}p < 0.05$ vs. paralytic stage. Scale bars in A-D = 20 μm.

Table 3 Histochemical evaluation of undiversified lectin binding patterns in rat olfactory mucosa induced EAE

Lectin	Olfactory mucosa			Lamina propria	
	Olfactory sensory neuron	Supporting cell	Basal cell	Nerve bundle	Bowman's gland
s-WGA	+++	+++	++	+++	+++
WGA	++	++	++	+++	++
DSL	+++	+++	+++	+++	+++
LEL	+++	+++	+++	+++	+++
STL	+++	+++	+/-	+++	+++
ConA	++	++	+	+	++
PSA	+++	++	+	+++	+/-
SBA	+++	+	++	+++	+++
SJA	-	-	-	-	++
RCA_{120}	+++	+++	++	+++	++
Jacalin	+++	+++	+	+++	++
PNA	+++	-	+/-	+	+++
ECA	+++	+++	++	++	+++
PHA-E	-	++	++	-	+
PHA-L	-	++	+	-	+++
UEA-I	++	++	+/-	+++	+++

–, negative staining; ±, faint staining; +, weak staining; ++, moderate staining; +++, intense staining.

4.4.2. LCA is up-regulated in the olfactory mucosa of EAE-affected rats among mannose binding lectins

The intensity of LCA expression in the basement membrane was increased in rats with paralytic-stage EAE (open arrows in Figure 9B) compared to normal control rats (Figure 9A) and was decreased in rats with recovery-stage EAE (Figure 9C). LCA histochemistry with 0.2 M MeαGlc showed no reactivity (Figure 9D).

A semi-quantitative comparison (Figure 9E) showed that the LCA-positive area in the olfactory mucosa of rats with paralytic-stage EAE was increased (25.09 ± 0.95%, $p < 0.05$) compared to that of normal control rats (19.29 ± 1.64%). The LCA-positive area was transiently and non-significantly downregulated in rats with recovery-stage EAE (22.76 ± 0.84%) compared to those with paralytic-stage EAE. The lectin-binding intensity of *Canavalia ensiformis* agglutinin and *Pisum sativum* agglutinin was similar in normal control rats and rats with EAE (Table 3).

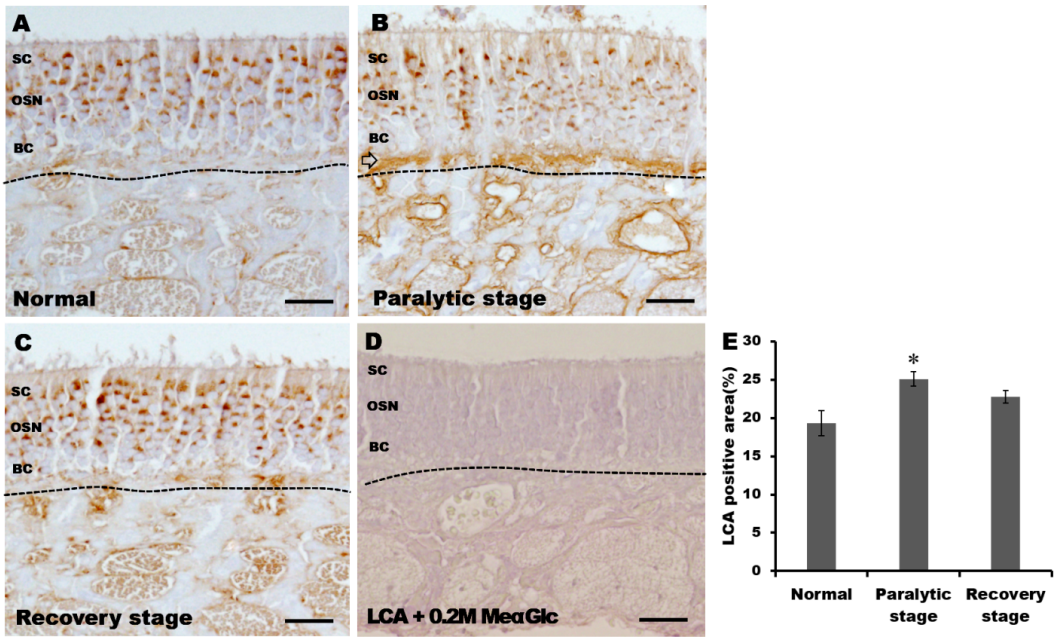

Figure 9. Histochemical analyses of LCA in the olfactory mucosa of (A) normal control, (B) paralytic-stage EAE, and (C) recovery-stage EAE rats. (A) In the normal control, LCA reactivity was labeled in olfactory sensory neurons, supporting cells, and basal cells. (B) At the paralytic stage, LCA binding intensity was upregulated in the basement membrane; (C) this tendency was maintained at the recovery stage. (D) Pre-incubation with 0.2 M MeαGlc as a negative control. No LCA reactivity was observed. (E) Semi-quantitative analysis of the LCA-positive area of the olfactory mucosa in normal control and EAE rats. LCA-positive area was measured above the dotted line. Open arrow, basement membrane; SC, supporting cell layer; OSN, olfactory sensory neuron layer; BC, basal cell layer. $^{*}p < 0.05$ vs. normal control. Scale bars in A-D = 20 μm.

4.4.3. VVA and DBA increase, but BSL-I decrease in the olfactory mucosa of EAE-affected rats among N-acetylgalactosamine-binding lectins

In normal control rats, VVA and DBA were labeled in the olfactory mucosa (Figure 10A and 10F). However, in rats with paralytic-stage EAE, the reactivities of VVA and DBA were more intensive for Bowman's gland (open arrowhead in Figure 10B) and the nuclei of supporting cells, olfactory sensory neurons, and basal cells (arrowhead, arrow, and open arrow in Figure 10G, respectively) compared to normal control rats. The labeling intensities of VVA and DBA slightly decreased in rats with recovery-stage EAE (Figure 10C and 10H). In a semi-quantitative comparison (Figure 10E and 10J), the VVA-positive area and the DBA-positive area in the lamina propria of rats with paralytic-stage EAE was significantly increased (6.86 ± 1.01%; VVA, 22.43 ± 1.53%; DBA, $p < 0.001$) compared to that of normal control rats (1.64 ± 0.19%; VVA, 7.51 ± 1.37%; DBA). There were no significant differences in VVA- and DBA-positive areas in rats with paralytic-stage EAE (5.39 ± 0.72%; VVA, 18.45 ± 2.83%; DBA) compared to those with paralytic-stage EAE. BSL-I expression in the olfactory sensory neuron layer and supporting cell layer was markedly downregulated in rats with paralytic-stage EAE (Figure 10L) compared to that in normal control rats (Figure 10K). In rats with recovery-stage EAE, BSL-I expression in the olfactory sensory neuron and supporting cell layer was similar to that of normal control rats (Figure 10M). The BSL-I-positive area in the olfactory mucosa of rats with paralytic-stage EAE was smaller (7.79 ± 0.51%, $p < 0.01$), than that of the control rats (13.7 ± 1.28%) (Figure 10O). The BSL-I-positive area was

restored in rats with recovery-stage EAE (11.41 ± 0.62%, $p < 0.05$ vs. paralytic stage, $p > 0.05$ vs. normal control). Pre-incubation with 0.2 M GalNAc in N-acetylgalactosamine-binding lectin histochemistry made lectin-reactivities abolished (Figure 10D, 10I and 10N). There were no differences in soybean agglutinin or *Sophora japonica* agglutinin reactivity between normal control rats and rats with EAE (Table 3).

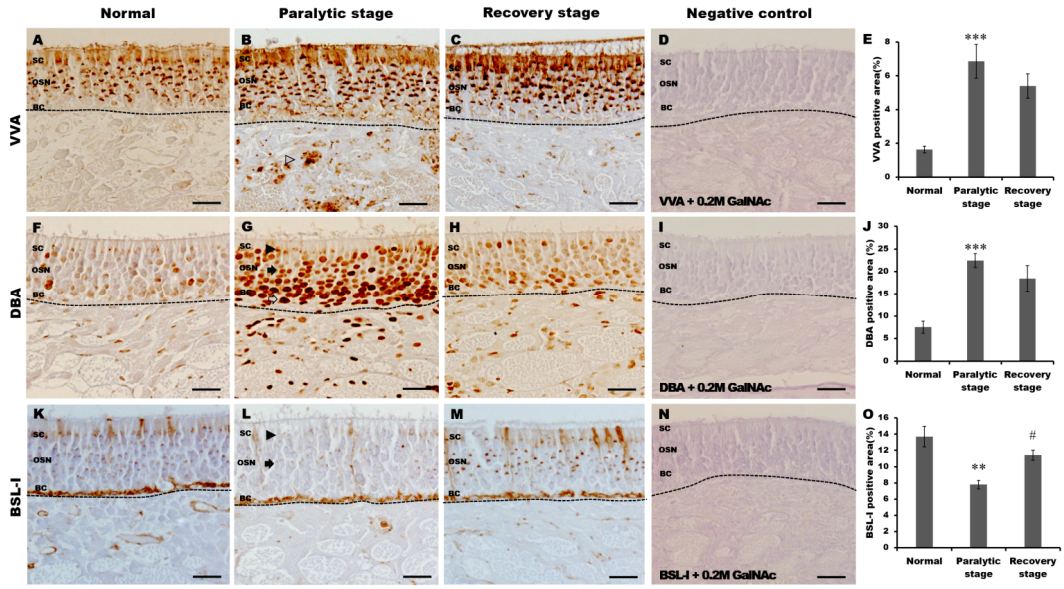

Figure 10. N-Acetylgalactosamine-binding lectin histochemistry in the olfactory mucosa of normal control (A, F and K), paralytic-stage EAE (B, G and L), and recovery-stage EAE (C, H and M) rats. In normal controls, (A) VVA reactivity was labeled in the olfactory mucosa, (F) DBA reactivity was weakly labeled in the olfactory mucosa, and (K) BSL-I reactivity was labeled in some olfactory sensory neurons and basal cell layer. VVA reactivity increased in all Bowman's glands at the paralytic (B) and recovery stages (C). (G) For all nuclei, DBA increased in the olfactory mucosa in the paralytic stage; (H) this tendency was maintained in the recovery stage. BSL-I reactivity markedly decreased in olfactory sensory neurons and supporting cells of the olfactory mucosa (L), and recovered to normal levels in the recovery stage (M). (D, I and N) Pre-incubation with 0.2 M GalNAc as a negative control. No lectin reactivity was observed. (E, J and O) Semi-quantitative analysis of VVA-, DBA-, and BSL-I-positive areas of the olfactory mucosa in normal control and EAE-affected rats. Lectin histochemistry for (A-E) VVA, (F-J) DBA, and (K-O) BSL-I. VVA-positive area was measured below the dotted line and DBA and

BSL-I-positive areas were measured above the dotted line. Arrowhead, supporting cell layer; arrow, olfactory sensory neuron layer; open arrowhead, Bowman's gland; open arrow, basal cell layer. $^{**}p < 0.01$, $^{***}p < 0.001$ vs. normal control, $^{\#}p < 0.05$ vs. paralytic stage. Scale bars (A-D, F-I and K-N) = 20 μm.

4.4.4. Galactose-binding lectins, complex type N-glycan-binding lectins and fucose-binding lectin are not significantly changed by EAE

The olfactory mucosa was labeled with galactose-binding lectins (*Ricinus communis* agglutinin, Jacalin, peanut agglutinin, and *Erythrina cristagalli* agglutinin) with various signal intensities, but the signal intensities did not differ between normal control rats and rats with EAE (Table 3).

Phytohemagglutinin-E and phytohemagglutinin-L showed reactivity with supporting cells and basal cells in normal control rats. The olfactory sensory neurons and nerve bundles did not show reactivity for phytohemagglutinin-E and phytohemagglutinin-L. The lectin-binding intensity did not differ between normal control rats and rats with EAE (Table 3). The fucose-binding lectin *Ulex europaeus* agglutinin-I showed various degrees of reactivity with the olfactory mucosa. However, *Ulex europaeus* agglutinin-I reactivity did not differ between normal control rats and rats with EAE (Table 3).

The changed lectin-binding patterns of the olfactory mucosa of rats with EAE are listed in Table 4.

Table 4 Summary of changed lectin binding patterns in EAE-affected rat compared with normal control

Lectin	Statement	Olfactory mucosa			Lamina propria	
		Olfactory sensory neuron	Supporting cell	Basal cell	Nerve bundle	Bowman's gland
BSL-II	Normal	++	++	±	-	+
	Paralysis	±	±	±	-	+
	Recovery	+	+	±	-	+
LCA	Normal	+++	+	+[a]	++	++
	Paralysis	+++	+	+++[a]	++	++
	Recovery	+++	+	+[a]	++	++
VVA	Normal	+++	+++	+	±	±
	Paralysis	+++	+++	+	±	+++
	Recovery	+++	+++	+	±	++
DBA	Normal	+	+	+	-	+
	Paralysis	+++	+++	+++	-	+++
	Recovery	++	++	++	-	++
BSL-I	Normal	++	++	+++	-	±
	Paralysis	±	+	+++	-	±
	Recovery	++	++	+++	-	±

–, negative staining; ±, faint staining; +, weak staining; ++, moderate staining; +++, intense staining.

a. In LCA histochemisty on basal cells, the degree of staining indicates the lectin-binding area of the basement membrane (lectin-positive intensity for basal cells were almost similar between normal and EAE-affected rat).

4.5. Double labeling of olfactory sensory neurons

Double immunofluorescence staining was performed to confirm whether BSL-I and BSL-II binding reactivities on olfactory sensory neurons decreased in rats with EAE. In the olfactory epithelium of normal control rats, some olfactory sensory neurons (arrows in Figure 11A and 11E) were labeled with both BSL-II and OMP/PGP 9.5 and BSL-II and OMP/PGP 9.5-double-positive area were respectively measured at 10.07 ± 1.46% for OMP (Figure 11D) and 10.99 ± 0.27% for PGP 9.5 (Figure 11H). However, in rats with paralytic-stage EAE, OMP/PGP 9.5-single positive olfactory sensory neurons were mostly detected (Figure 11B and 11F) and double-positive area were decreased (Figure 11D, 1.55 ± 0.33%, $p < 0.001$ vs. normal control; Figure 11H, 1.75 ± 0.71%, $p < 0.001$ vs. normal control). BSL-II and OMP/PGP 9.5-double labeled olfactory neurons (arrows in Figure 11C and 11G) were detected and double-positive area were recovered at 5.72 ± 1.02% for OMP (Figure 11D, $p < 0.01$ vs. paralytic-stage EAE) and 5.27 ± 0.88% for PGP 9.5 (Figure 11H, $p < 0.05$ vs. paralytic-stage EAE).

In double immunofluorescence staining with BSL-I and OMP/PGP 9.5, basal cell layer and some olfactory sensory neurons were co-localized (arrows and arrowheads in Figure 11I and 11M, respectively) and double-positive area were measured 11.73 ± 1.07% for OMP (Figure 11L) and 9.90 ± 0.60% for PGP 9.5 (Figure 11P) in normal control rats. In rats with paralytic-stage EAE, few olfactory sensory neurons double-labeled with BSL-I and OMP/PGP 9.5 was detected (Figure 11J and 11N) and

double-positive area were decreased (Figure 11L, 5.56 ± 0.34%, $p < 0.01$ vs. normal control; Figure 11P, 5.5 ± 0.29%, $p < 0.01$ vs. normal control). However, in rats with recovery-stage EAE, the number of BSL-I and OMP/PGP 9.5 double-labeled olfactory sensory neurons (arrows in Figure 11K and 11O) was increased and double-positive area was recovered to the level of those of normal control rats (Figure 11L, 10.24 ± 1.73%, $p < 0.05$ vs. paralytic-stage EAE; Figure 11P, 9.27 ± 0.64%, $p < 0.01$ vs. paralytic-stage EAE).

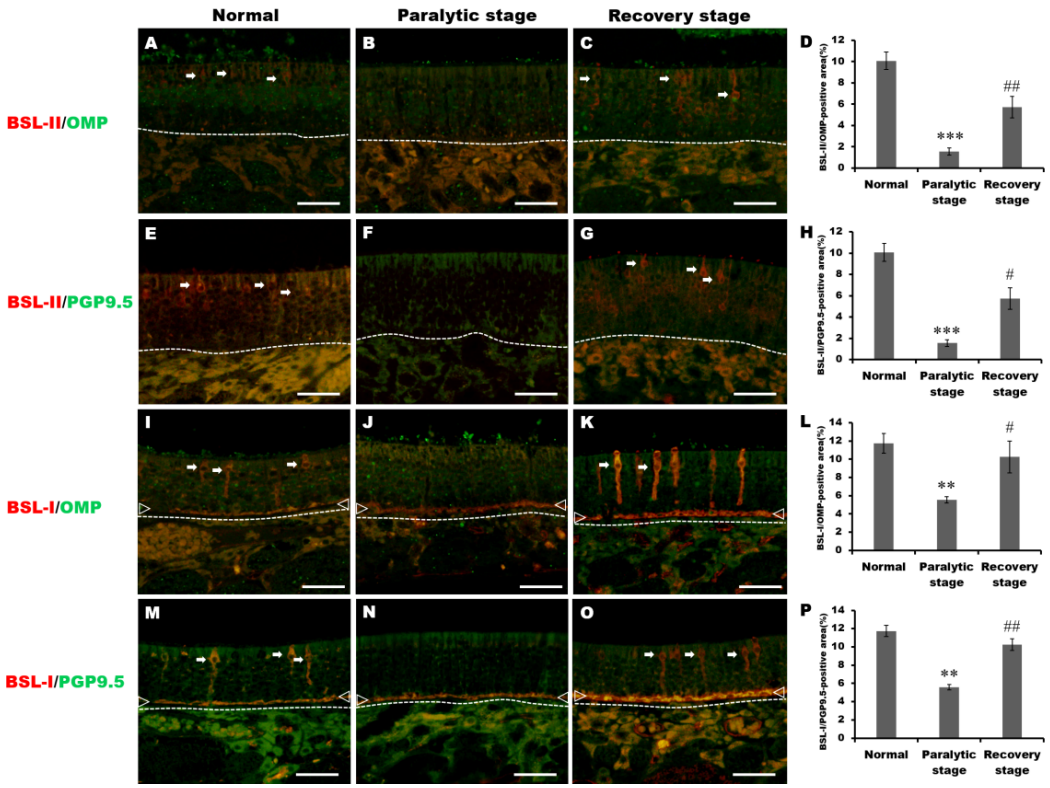

Figure 11. Double immunofluorescence reactivities to lectins (BSL-II and BSL-I; red) and to antibodies (OMP and PGP 9.5; green) in the olfactory mucosa of normal control and EAE-affected rats. Arrows indicate the co-localization of lectins and antibodies to olfactory sensory neurons. Arrowheads, co-localization of lectins and antibodies in the basal cell layer. Double-positive area was measured above dotted line. (D, H, L and P) Bar graphs show a semi-quantitative analysis for lectins and antibodies-double-positive area of the olfactory mucosa in normal and EAE-affected rats. $^{**}p< 0.01$, $^{***}p< 0.001$ vs. normal control, $^{\#}p< 0.05$, $^{\#\#}p< 0.01$ vs. paralytic stage. Scale bars = 20 μm.

5. Discussion

This is the first report that CNS inflammation in EAE affects not only the olfactory bulb by inducing microglial reaction and astrogliosis (Kim et al., 2018) but also the olfactory mucosa by changing its glycan expression. We observed downregulated glycan expression in the olfactory sensory neurons and glycan upregulation in several components of the olfactory mucosa. These findings suggest that glycan expression changes may be used as an indicator of CNS inflammation in the olfactory mucosa.

Olfactory dysfunction is an early clinical manifestation of neurodegenerative diseases; therefore, olfactory impairment can be used as a marker of CNS inflammation (Doty, 2017). In some animal models of neurodegenerative disease such as Niemann–Pick type C1 mutant mice and APP/PS1 transgenic mice, the olfactory mucosa is damaged, causing olfactory dysfunction (Hovakimyan et al., 2013; Yao et al., 2017). In EAE-affected rats, inflammatory cells in the olfactory mucosa originate from two routes: (1) migration of inflammatory cells from the olfactory bulb and olfactory nerve (Kaminski et al., 2012; Kim et al., 2018; Kim et al., 2019) and (2) activation of olfactory mucosa immune cells via the flow of inflammatory cytokines produced in the CNS through cerebrospinal fluid and blood circulation (Chen et al., 2015). These inflammatory cells do not induce olfactory sensory neuronal loss, but may cause transient olfactory dysfunction.

Glycans are required for glycosylation of glycolipids and glycoproteins and play important roles in the nervous system; e.g., in

cell/cell interactions, signaling, and proliferation (Kleene and Schachner, 2004). In the olfactory system, glycans participate in the proliferation and development of olfactory cells and the sensing and processing of odorant information (Plendl and Sinowatz, 1998). Glycans can be modified in the presence of inflammation; e.g., Aβ25-35 induces overexpression of mucin-type O-glycosylated proteins and 9-O-acetylated sialic acid moieties with neuro-inflammation in rats (Limon et al., 2011; Ramos-Martinez et al., 2018). In diabetic retinopathy, hyperglycemia-induced inflammatory reactions upregulate N-glycosylation in the retinal vessel and stimulate the expression of intercellular adhesion molecule-1 (Liu et al., 2016). Thus, glycan expression is modified in the presence of inflammation and so EAE may influence the glycan expression profile of the olfactory mucosa.

In this study, glycan expression was altered in rats with paralytic-stage EAE; glycans with altered expression differed among olfactory mucosa components. Olfactory sensory neurons extend dendritic terminals containing specific glycan epitopes (Foster et al., 1992; Takami et al., 1995); olfaction is thought to be initiated following recognition of odorant molecules through the olfactory sensory neuron glycan epitope (Breer, 1991; Kalinoski et al., 1987). We postulated that downregulation of BSL-I and -II in olfactory sensory neurons could be related to transient olfactory dysfunction by inhibiting the recognition of odorant molecules containing N-acetyl-glucosamine or N-acetyl-galactose epitope. Because glycans are upregulated in diverse pathologies (Limon et al., 2011; Liu et al., 2016; Ramos-Martinez et al., 2018), increased LCA, VVA or DBA reactivity may be involved in the olfactory mucosa immune response against CNS inflammation.

Glycan expression is also altered during aging. For example, in mice, α1–2 fucose glycan expression in olfactory sensory neurons and the glomeruli of the main olfactory bulb increases with age (Kondoh et al., 2018). Therefore, the undiversified lectins in the olfactory mucosa of rats with EAE may be not related to CNS inflammation.

Collectively, our findings (summarized in Figure 12) suggest that the levels of most glycans are not altered in the olfactory mucosa of rats with EAE and CNS inflammation, but the levels of some glycans are modulated. Because olfactory dysfunction in animals with EAE is transient (Kim et al., 2018), glycans whose expression is altered in the paralytic stage might bind to or transfer odorant molecules, leading to olfactory dysfunction. The function of these glycans warrants further study.

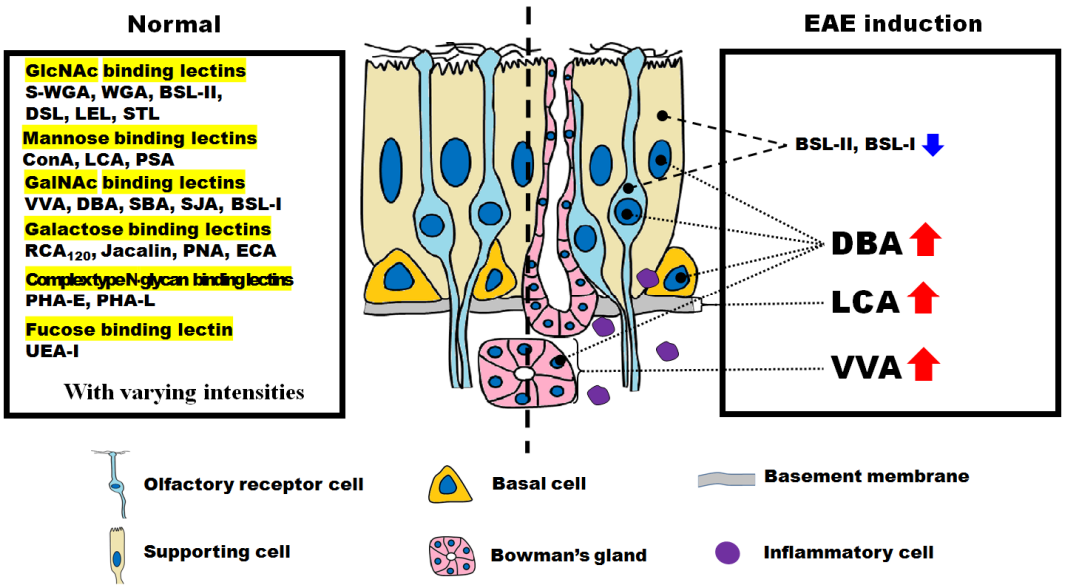

Figure 12. Diagram showing changes in lectin-binding patterns in the olfactory mucosa of rats with EAE. Reactivity increased in the olfactory mucosa of paralytic-stage EAE rats for basement-membrane LCA, Bowman's gland VVA, and DBA in all nuclei; BSL-II and BSL-I reactivity olfactory sensory neurons and supporting cells decreased. GlcNAc, N-acetylglucosamine; GalNAc, N-acetylgalactosamine.

References

Ahn, M., Yang, W., Kim, H., Jin, J.K., Moon, C., Shin, T., 2012. Immunohistochemical study of arginase-1 in the spinal cords of Lewis rats with experimental autoimmune encephalomyelitis. Brain Res. 1453**,** 77-86.

Breer, H., 1991. Molecular reaction cascades in olfactory signal transduction. J Steroid Biochem Mol Biol. 39**,** 621-5.

Caminiti, F., De Salvo, S., De Cola, M.C., Russo, M., Bramanti, P., Marino, S., Ciurleo, R., 2014. Detection of olfactory dysfunction using olfactory event related potentials in young patients with multiple sclerosis. PLoS One. 9**,** e103151.

Chen, L., Elias, G., Yostos, M.P., Stimec, B., Fasel, J., Murphy, K., 2015. Pathways of cerebrospinal fluid outflow: a deeper understanding of resorption. Neuroradiology. 57**,** 139-47.

Doty, R.L., 2017. Olfactory dysfunction in neurodegenerative diseases: is there a common pathological substrate? Lancet Neurol. 16**,** 478-88.

Foster, J.D., Getchell, M.L., Getchell, T.V., 1992. Ultrastructural localization of sialylated glycoconjugates in cells of the salamander olfactory mucosa using lectin cytochemistry. Cell Tissue Res. 267**,** 113-24.

Hovakimyan, M., Meyer, A., Lukas, J., Luo, J., Gudziol, V., Hummel, T., Rolfs, A., Wree, A., Witt, M., 2013. Olfactory deficits in

Niemann-Pick type C1 (NPC1) disease. PLoS One. 8, e82216.

Ichikawa, M., Takami, S., Osada, T., Graziadei, P.P., 1994. Differential development of binding sites of two lectins in the vomeronasal axons of the rat accessory olfactory bulb. Brain Res Dev Brain Res. 78, 1-9.

Kalinoski, D.L., Bruch, R.C., Brand, J.G., 1987. Differential interaction of lectins with chemosensory receptors. Brain Res. 418, 34-40.

Kaltner, H., Stippl, M., Knaus, M., El-Matbouli, M., 2007. Characterization of glycans in the developmental stages of Myxobolus cerebralis (Myxozoa), the causative agent of whirling disease. J Fish Dis. 30, 637-47.

Kaminski, M., Bechmann, I., Pohland, M., Kiwit, J., Nitsch, R., Glumm, J., 2012. Migration of monocytes after intracerebral injection at entorhinal cortex lesion site. J Leukoc Biol. 92, 31-9.

Kim, J., Choi, Y., Ahn, M., Jung, K., Shin, T., 2018. Olfactory Dysfunction in Autoimmune Central Nervous System Neuroinflammation. Mol Neurobiol. 55, 8499-508.

Kim, J., Ahn, M., Choi, Y., Ekanayake, P., Park, C.M., Moon, C., Jung, K., Tanaka, A., Matsuda, H., Shin, T., 2019. Gene Expression Profile of Olfactory Transduction Signaling in an Animal Model of Human Multiple Sclerosis. Exp Neurobiol. 28, 74-84.

Kleene, R., Schachner, M., 2004. Glycans and neural cell interactions. Nat

Rev Neurosci. 5, 195-208.

Kondoh, D., Sasaki, M., Kitamura, N., 2018. Age-dependent decrease in glomeruli and receptor cells containing alpha1-2 fucose glycan in the mouse main olfactory system but not in the vomeronasal system. Cell Tissue Res. 373, 361-6.

Lee, K.H., Park, C., Kim, J., Moon, C., Ahn, M., Shin, T., 2016. Histological and lectin histochemical studies of the vomeronasal organ of horses. Tissue Cell. 48, 361-9.

Limon, I.D., Ramirez, E., Diaz, A., Mendieta, L., Mayoral, M.A., Espinosa, B., Guevara, J., Zenteno, E., 2011. Alteration of the sialylation pattern and memory deficits by injection of Abeta(25-35) into the hippocampus of rats. Neurosci Lett. 495, 11-6.

Lipscomb, B.W., Treloar, H.B., Klenoff, J., Greer, C.A., 2003. Cell surface carbohydrates and glomerular targeting of olfactory sensory neuron axons in the mouse. J Comp Neurol. 467, 22-31.

Liu, K., Liu, H., Zhang, Z., Ye, W., Xu, X., 2016. The role of N-glycosylation in high glucose-induced upregulation of intercellular adhesion molecule-1 on bovine retinal endothelial cells. Acta Ophthalmol. 94, 353-7.

Melgarejo Moreno, P., Hellin Meseguer, D., Melgarejo Moreno, C., 1998. [Olfactory epithelium of the rat. Lectin-mediated histochemical studies]. An Otorrinolaringol Ibero Am. 25, 471-80.

Oikawa, T., Saito, H., Taniguchi, K., Taniguchi, K., 2001. Immunohistochemical studies on the differential maturation of three types of olfactory organs in the rats. J Vet Med Sci. 63, 759-65.

Patel, R.M., Pinto, J.M., 2014. Olfaction: anatomy, physiology, and disease. Clin Anat. 27, 54-60.

Plendl, J., Schmahl, W., 1988. Dolichos biflorus agglutinin: a marker of the developing olfactory system in the NMRI-mouse strain. Anat Embryol (Berl). 177, 459-64.

Plendl, J., Sinowatz, F., 1998. Glycobiology of the olfactory system. Acta Anat (Basel). 161, 234-53.

Ramos-Martinez, I., Martinez-Loustalot, P., Lozano, L., Issad, T., Limon, D., Diaz, A., Perez-Torres, A., Guevara, J., Zenteno, E., 2018. Neuroinflammation induced by amyloid beta25-35 modifies mucin-type O-glycosylation in the rat's hippocampus. Neuropeptides. 67, 56-62.

Saito, H., Ogawa, K., Taniguchi, K., 1994. [Lectin-binding patterns of the olfactory receptors (olfactory epithelium, vomeronasal organ and septal olfactory organ of Masera) in the rat]. Jikken Dobutsu. 43, 51-60.

Salazar, I., Sanchez-Quinteiro, P., Lombardero, M., Cifuentes, J.M., 2000. A descriptive and comparative lectin histochemical study of the vomeronasal system in pigs and sheep. J Anat. 196 (Pt 1), 15-22.

Shin, T., Ahn, M., Matsumoto, Y., 2012. Mechanism of experimental autoimmune encephalomyelitis in Lewis rats: recent insights from macrophages. Anat Cell Biol. 45**,** 141-8.

Shin, T., Kim, J., Choi, Y., Ahn, M., 2017. Glycan diversity in the vomeronasal organ of the Korean roe deer, Capreolus pygargus: A lectin histochemical study. Acta Histochem. 119**,** 778-85.

Shin, T., Kim, J., Ahn, M., Moon, C., 2018. Olfactory Dysfunction in CNS Neuroimmunological Disorders: a Review. Mol Neurobiol. 56, 3714-21.

Takami, S., Getchell, M.L., Getchell, T.V., 1995. Resolution of sensory and mucoid glycoconjugates with terminal alpha-galactose residues in the mucomicrovillar complex of the vomeronasal sensory epithelium by dual confocal laser scanning microscopy. Cell Tissue Res. 280**,** 211-6.

Yao, Z.G., Hua, F., Zhang, H.Z., Li, Y.Y., Qin, Y.J., 2017. Olfactory dysfunction in the APP/PS1 transgenic mouse model of Alzheimer's disease: Morphological evaluations from the nose to the brain. Neuropathology. 37**,** 485-94.

Abstract in Korean

실험적 자가면역성 뇌척수염을 유도한 쥐에서 후각점막의 당사슬 변화

(지도교수 : 신 태 균)

박 창 남

제주대학교 일반대학원 수의학과

당사슬은 당접합체의 탄수화물기로 분자학적 구조, 당의 성분 및 결합 특이성에 따라 구분된다. 특히, 신경계의 후각기계에서 후각신경뉴런의 발달과 증식, 시냅스 형성, 냄새 신호 처리에 중요한 역할을 맡으며, 동물 종, 발생단계, 노화에 따라 발현에 차이가 있다고 알려져 있다. 그러나 신경염증 상태에서 후각기계의 당사슬 변화에 대해서는 밝혀진 바가 없다.

본 연구에서는 실험적 자가면역성 뇌척수염 (experimental autoimmune encephalomyelitis, EAE)을 유도한 쥐에서 염증세포의 대표적인 지표물질인 ionized calcium-binding adaptor molecule-1 (Iba-1) 항체를 이용한 면역조직화학법과 21종 렉틴을 이용한 조직화학법을 수행하여 중추신경 내에 발생한 염증이 후각점막에 미치는 영향을 정상대조군, 마비기, 회복기의 실험동물을 이용하여 평가하였다.

면역조직화학적 평가에서는 실험적 자가면역성 뇌척수염을 유도한 후 마비증세를 보이는 실험군의 척수를 비롯한 중추신경계와 후각점막에서 Iba-1 발현이 정상대조군보다 유의적으로 증가하였으며, 이후 회복기에서 정상대조군 수준으로 발현이 감소하였다. 이를 통해 자가면역성 뇌척수염을 유도한 쥐에서 중추신경계 내에 발생한 염증이 말초의 후각점막으로

이동된다는 사실을 확인하였다.

정상대조군과 실험적 자가면역성 뇌척수염 유도군간 렉틴 조직화학염색을 비교한 결과, 16종의 렉틴은 후각감각뉴런, 지지세포, 바닥세포, 신경다발, 보우만샘에서 특이적인 차이를 보이지 않았으나, 5종의 렉틴은 마비기의 실험적 자가면역성 뇌척수염 유도군 후각점막에서 정상대조군과 비교하였을 때 유의성 있는 증감을 나타내었다. *Bandeiraea simplica* lectin (BSL)-I과 BSL-II는 마비기 실험적 자가면역성 뇌척수염 유도군에서 후각신경세포과 지지세포에서 유의적으로 발현이 감소한 후 회복되는 경향을 나타내었다. 이에 반해, *Lens culinaris* agglutinin (LCA), *Vicia villosa* agglutinin (VVA), *Dolichos biflorus* agglutinin (DBA)는 각각 바닥막, 보우만샘, 모든 세포의 핵 내에서 발현이 유의적으로 증가하였다. 증가된 LCA, VVA, DBA는 회복기에 정상대조군과 비슷한 수준으로 발현하였다.

본 연구를 통해 실험적 자가면역성 뇌척수염을 유발시킨 쥐에서 중추신경염증이 후각점막에 염증반응을 일으킬 수 있으며, 후각점막 내 일부 당사슬 발현에 변화를 일으킬 수 있음을 확인하였다. 마비기 실험적 자가면역성 뇌척수염 유도군의 후각신경세포 내 BSL-II와 BSL-I의 발현감소는 N-acetyl-glucosamine과 N-acetyl-galactosamine로 인식 가능한 냄새 분자 감지에 장애를 일으켜 일시적인 후각장애를 일으킬 것으로 예상되며, 증가한 LCA, VVA, DBA 발현은 후각점막의 면역반응과 연관될 것으로 추정된다.

주요어: 실험적 자가면역성 뇌척수염, 후각점막, 렉틴, 당사슬.

감사의 글

석사학위를 마치고 먹고사는 문제를 해결하던 중, 마음 구석에는 항상 학문에 대한 미련이 남아있었습니다. 한번뿐인 인생 후회하고 싶지 않아 박사학위 과정을 선택했고, 어쩌다보니 벌써 졸업을 앞두게 되었습니다. 학위과정이 결코 쉽지 않았으나, 즐겁고 감사한 기억을 담아 저에게 가르침과 격려를 보내주셨던 분들에게 감사한 말씀을 드리려 합니다.

우선 대부이자 스승이신 신태균 교수님께 감사드립니다. 교수님 지도가 있어 학문의 즐거움을 깨달았고, 몸소 가르쳐주신 '근성'과 '프로정신'은 삶을 살아가는 큰 버팀목이 됩니다. 그리고 학위과정 중 여러 번 넘어졌던 저를 일으켜준 김정태 교수님, 물심양면으로 인생의 조언을 해주신 이광협 원장님, 학위과정을 시작할 수 있게 북돋워주신 양형석 팀장님, 학위논문완성에 많은 조언과 가르침을 주신 강태영 교수님께 감사의 말씀 올립니다.

실험실 생활동안 아낌없는 격려를 보내주신 이용덕 박사님, 김승준 교수님, 강재윤 선배님, 김황룡 선배님, 진재광 박사님, 문창종 교수님, 강종철 선배님, 허승담 선배님, 안미정 교수님, 이기현 선배님, 김희철 박사님, 정경숙 선배님, 정찬우 선배님, 정진우 선배님께 진심으로 감사드립니다. 그리고 학위과정동안 희노애락을 함께한 고현주 선배님, 원준형, 유나, 전지윤 선생님에게 고마운 마음을 전합니다.

끝으로 지금의 제가 설 수 있도록 바탕이 되어주신 부모님, 힘든 시간을 같이 보내준 동생 용남, 가까이서 응원해주신 장인·장모님, 평생을 함께 할 동반자 민진이, 아들 인한에게 감사의 말을 남깁니다.